

Diffusion Epistemic Uncertainty with Asymmetric Learning for Diffusion-Generated Image Detection

Yingsong Huang^{1*}, Hui Guo^{1*}, Jing Huang^{2*}, Bing Bai^{3†} and Qi Xiong^{1†}

¹Tencent Inc. ²Hikvision ³Microsoft MAI

{hudsonhuang, emmaguo}@tencent.com, huangjing29@hikvision.com
bingbai@microsoft.com, keonxiong@tencent.com

Abstract

The rapid progress of diffusion models highlights the growing need for detecting generated images. Previous research demonstrates that incorporating diffusion-based measurements, such as reconstruction error, can enhance the generalizability of detectors. However, ignoring the differing impacts of aleatoric and epistemic uncertainty on reconstruction error can undermine detection performance. Aleatoric uncertainty, arising from inherent data noise, creates ambiguity that impedes accurate detection of generated images. As it reflects random variations within the data (e.g., noise in natural textures), it does not help distinguish generated images. In contrast, epistemic uncertainty, which represents the model’s lack of knowledge about unfamiliar patterns, supports detection. In this paper, we propose a novel framework, Diffusion Epistemic Uncertainty with Asymmetric Learning (DEUA), for detecting diffusion-generated images. We introduce Diffusion Epistemic Uncertainty (DEU) estimation via the Laplace approximation to assess the proximity of data to the manifold of diffusion-generated samples. Additionally, an asymmetric loss function is introduced to train a balanced classifier with larger margins, further enhancing generalizability. Extensive experiments on large-scale benchmarks validate the state-of-the-art performance of our method.

1. Introduction

The rapid advancement of diffusion models [13, 20, 22, 43, 48, 50] has enabled the generation of images that are nearly indistinguishable from real ones to the human eye. This raises concerns about potential misuse of generated images in various fields, such as security risks and privacy violations [24]. Consequently, there is an increasing need for effective methods to detect diffusion-generated images.

*These authors contributed equally to this work.

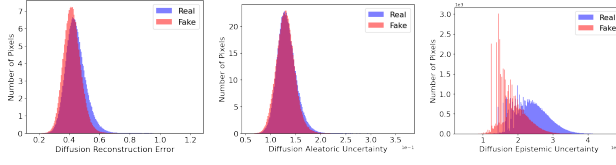
†Corresponding authors.

Recent approaches have proposed using diffusion measurements, such as reconstruction error [38, 39, 55], as discriminative features for detecting diffusion-generated images. These methods assume that images generated by the diffusion model and their corresponding reconstructions share the same distribution. As a result, pre-trained diffusion models can reconstruct generated images more accurately, whereas the reconstruction error for real images is typically larger.

However, large reconstruction errors are not solely caused by out-of-distribution (OOD) data. Both aleatoric and epistemic uncertainty, inherent in the diffusion [3], contribute to reconstruction error. Aleatoric uncertainty reflects the inherent noise and randomness in the data. As it remains relatively constant across both in-distribution and OOD samples [25], it does not significantly aid in detecting diffusion-generated images. This insight motivates a shift from reconstruction error towards epistemic uncertainty.

Epistemic uncertainty, in contrast, captures the model’s lack of knowledge about unfamiliar patterns and increases significantly for samples that fall outside the domain of the training data [12, 23, 25, 40]. Consequently, epistemic uncertainty provides a more reliable basis for anomaly detection. Figure 1 demonstrates that epistemic uncertainty more accurately distinguishes real samples from fake ones. Therefore, for detecting generated images, it is essential to disentangle the overall uncertainty in diffusion measurements and focus specifically on epistemic uncertainty.

Based on this insight, we propose Diffusion Epistemic Uncertainty with Asymmetric Learning (DEUA), a novel framework for detecting diffusion-generated images. Our framework separates overall uncertainty into aleatoric and epistemic components, using Diffusion Epistemic Uncertainty (DEU) to identify samples close to the manifold of diffusion-generated images. We employ the last-layer Laplace approximation [10, 28] to estimate epistemic uncertainty in the diffusion process. Moreover, during the training of a classifier, we observe a phenomenon akin to the “sink class” concept, where there is asymmetric separa-



(a) Distribution of reconstruction error. (b) Distribution of aleatoric uncertainty. (c) Distribution of epistemic uncertainty.

Figure 1. Distribution of diffusion reconstruction error, aleatoric uncertainty, and epistemic uncertainty in real and generated samples. (a) The reconstruction error distribution for real samples overlaps with that of fake samples due to the presence of aleatoric uncertainty. (b) The distribution of aleatoric uncertainty is nearly indistinguishable between real and fake samples. (c) Epistemic uncertainty more accurately distinguishes real samples from fake ones.

tion between the real and fake classes [44]. To address this, we introduce an asymmetric contrastive loss function that aims to train a classifier with a balanced decision boundary and larger margins, thus improving its generalizability.

The key contributions of this work are summarized as follows:

- We analyze why the use of diffusion reconstruction error in existing methods is insufficient for detecting generated images and identify the predictive ambiguity introduced by aleatoric uncertainty.
- We introduce a novel framework for detecting diffusion-generated images, leveraging diffusion epistemic uncertainty to identify samples close to the manifold of generated images, and using asymmetric contrastive learning to train a classifier with enhanced generalizability.
- Extensive experiments on large-scale datasets, namely GenImage and DRCT-2M, validate the effectiveness of the proposed framework.

2. Related Work

In this section, we review related work on generalizable generated image detection and uncertainty estimation in diffusion.

2.1. Generalizable Generated Image Detection

In recent years, research on detecting AI-generated images has evolved from hunting for obvious artifacts to probing increasingly subtle statistical cues. Early studies targeted visible flaws—including abnormal color [41], lighting inconsistencies [14], texture anomalies [36], and blending seams [32]—but such errors have largely disappeared as generators improve. Accordingly, the community shifted to fine-grained spatial [4, 18, 52] and spectral signatures [16, 45, 54, 61], work that was initially developed for GAN imagery [33]. Subsequent studies revealed that diffusion models also leave tell-tale spectral traces [6, 7], while NPR [53] exploited local pixel dependencies created

by up-sampling modules, capturing both GAN and diffusion fakes. To bolster cross-model generalization, several approaches embed or fuse local forgery evidence within CLIP’s vision-language space [8, 44, 49] or jointly reason over spatial-frequency domains, as in FatFormer and AIDE [35, 58]. A parallel line of work leverages the pretrained diffusion model itself: DIRE [55] and SeDID [39] rely on reconstruction error, DNF [62] analyzes predicted noise during inversion, and LaRE² [38] achieves similar benefits with a single-step latent error, all building on the premise that synthetic images are more faithfully reconstructed than real ones. We argue that randomness in the forward diffusion process introduces prediction ambiguity and instead measure *epistemic uncertainty*—how unsure the model is about its own predictions—to gauge a sample’s proximity to the synthetic manifold. Concurrently, multimodal large models such as ForgeryGPT [31] and HEIE [59] provide interpretable detection via cross-modal or chain-of-thought reasoning, and a new wave of zero-/few-shot methods (e.g., ZED [9], FSD [56]) achieves robustness to unseen generators without extensive synthetic data.

Against this backdrop, our work delves into the generation process itself and introduces a diffusion-based epistemic-uncertainty metric that complements reconstruction- and entropy-based criteria, offering a principled, source-agnostic signal for detecting AI-generated images.

2.2. Uncertainty Estimation and Laplace Approximation

Probabilistic modeling methods, such as Bayesian Neural Networks (BNNs) [17, 40] and deep ensembles [29] have demonstrated the ability to estimate uncertainty. BNNs place a prior distribution over the model parameters and quantify uncertainty as the sample variance over the weight distribution. Deep ensembles train an ensemble of networks with different weight initializations and take the ensemble variance as a measure of uncertainty.

Due to BNNs’ high nonlinearity, it is infeasible to analytically compute the Bayesian posterior of parameters. Approximate inference techniques, such as variational inference (VI) [1] and Laplace approximation (LA) [47] are introduced to establish an approximation of the posterior. LA can be effortlessly applied to pre-trained models in a post-processing manner and has strong uncertainty quantization performance [10, 15].

Recently, there has been some exploration around uncertainty estimation in diffusion [3, 27]. Our estimation method is related to BayesDiff [27]. The main difference is that our method qualifies the uncertainty in the forward and reverse diffusion process on existing images while BayesDiff focuses on characterizing the uncertainty in the reverse diffusion process on images to be generated.

3. Preliminaries

In this section, we review the forward and reverse diffusion processes. We then examine the influence of two types of uncertainty on the detection of generated images, and present case studies to illustrate these concepts. Additionally, we briefly introduce the Laplace approximation for efficient Bayesian inference in diffusion. We use it to estimate epistemic uncertainty in Sec. 4.2.

3.1. Diffusion Model

A diffusion model typically involves two processes. The forward process defines a Markov chain of steps that gradually add Gaussian noise to the raw image \mathbf{x}_0 until degenerating it into isotropic Gaussian distribution, which is defined as:

$$q(\mathbf{x}_t | \mathbf{x}_{t-1}) = \mathcal{N}(\mathbf{x}_t; \sqrt{\frac{\alpha_t}{\alpha_{t-1}}} \mathbf{x}_{t-1}, (1 - \frac{\alpha_t}{\alpha_{t-1}} \mathbf{I})), \quad (1)$$

where \mathbf{x}_t is the noisy image at the t -th step, α_t is a predefined noise schedule, and T is the total steps. According to the property of Markov chain, we can get \mathbf{x}_t from \mathbf{x}_0 via:

$$q(\mathbf{x}_t | \mathbf{x}_0) = \mathcal{N}(\mathbf{x}_t; \sqrt{\alpha_t} \mathbf{x}_0, (1 - \alpha_t) \mathbf{I}). \quad (2)$$

The reverse process is also formulated as a Markov chain in DDPM [22], using a network $p_\theta(\mathbf{x}_{t-1} | \mathbf{x}_t)$ to fit the real distribution $q(\mathbf{x}_{t-1} | \mathbf{x}_t)$:

$$p_\theta(\mathbf{x}_{t-1} | \mathbf{x}_t) = \mathcal{N}(\mathbf{x}_{t-1}; \boldsymbol{\mu}_\theta(\mathbf{x}_t, t), \boldsymbol{\Sigma}_\theta(\mathbf{x}_t, t)). \quad (3)$$

In practice, the optimization target is simplified to predicting the added noise ϵ as another parameterization of $p_\theta(\mathbf{x}_{t-1} | \mathbf{x}_t)$.

To accelerate the iterative process, DDIM [50] proposes a new deterministic method without the Markov hypothesis. The new reverse process is formulated as:

$$\begin{aligned} \mathbf{x}_{t-1} = \sqrt{\alpha_{t-1}} & \left(\frac{\mathbf{x}_t - \sqrt{1 - \alpha_t} \epsilon_\theta(\mathbf{x}_t, t)}{\sqrt{\alpha_t}} \right) + \\ & \sqrt{1 - \alpha_{t-1} - \sigma_t^2} \epsilon_\theta(\mathbf{x}_t, t) + \sigma_t \epsilon_t. \end{aligned} \quad (4)$$

With the formulation, the reverse process become deterministic if $\sigma_t = 0$. Moreover, DDIM proposes to sample a subset of S steps τ_1, \dots, τ_S , and thus the reverse process can generate samples following the new faster schedule.

3.2. Rethink Uncertainty in the Diffusion Process

Uncertainty can have a significant impact on the reconstruction error commonly used in diffusion-generated image detection [3], where aleatoric and epistemic components can lead to prediction ambiguity. Distinguishing between these two forms of uncertainty is essential for accurately detecting diffusion-generated images, as they affect the detection process in fundamentally different ways.

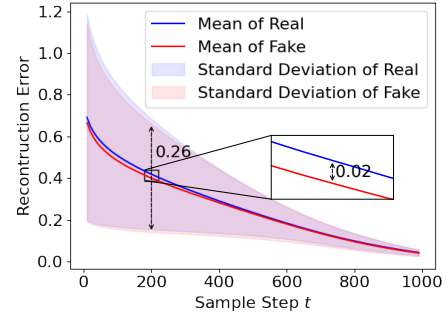


Figure 2. Diffusion Reconstruction error and predictive ambiguity (1000 images are used) due to aleatoric uncertainty. The difference in reconstruction error becomes less significant when compared to the standard deviation caused by aleatoric uncertainty.

Aleatoric uncertainty arises from inherent noise in the observed data and reflects aspects of the task that are intrinsically difficult [17, 25]. For instance, image patches with high-frequency details or complex natural textures often exhibit greater aleatoric uncertainty during the diffusion reconstruction process. Notably, aleatoric uncertainty does not increase for out-of-distribution (OOD) samples, making it unsuitable for detecting such anomalies. Moreover, relying on diffusion-based measurements (e.g., reconstruction error) to identify generated images can become misleading when aleatoric uncertainty dominates, as it inflates prediction ambiguity. Figure 2 illustrates how aleatoric uncertainty causes predictive ambiguity in reconstruction error estimates. Specifically, the reconstruction error is computed as the mean of sampled diffusion errors, while aleatoric uncertainty is estimated via the sample variance. To ensure robust statistics, we use a set of 1,000 images, each sampled 20 times, and take the mean across all pixels. Although there is a notable gap between the mean reconstruction errors of real and fake images, the standard deviation introduced by aleatoric uncertainty diminishes this difference. Consequently, as shown in Fig. 1a, relying solely on reconstruction error is less effective for distinguishing real from fake images when aleatoric uncertainty is high.

By contrast, epistemic uncertainty captures the model’s lack of knowledge about unfamiliar patterns, increasing significantly for samples far outside the training distribution [25]. This property makes epistemic uncertainty more reliable for identifying diffusion-generated images. This is also validated in Fig. 1c, where epistemic uncertainty more accurately distinguishes real samples from fake ones.

3.3. Laplace Approximation for Bayesian Diffusion Models

To capture epistemic uncertainty, we turn the deterministic neural network $\epsilon_\theta(\mathbf{x}_t, t)$ into a Bayesian Neural Network (BNN) by assuming an isotropic Gaussian prior $p(\theta)$.

Let \mathcal{D} be the training dataset, the target of Bayesian inference is to infer the posterior $p(\theta|\mathcal{D})$ and predict distribution of noise for noise-corrupted data \mathbf{x}_t^* with

$$p(\epsilon_t^*|\mathbf{x}_t^*, \mathcal{D}) = \int p(\epsilon|\epsilon_\theta(\mathbf{x}_t^*, t))p(\theta|\mathcal{D})d\theta. \quad (5)$$

Since $p(\theta|\mathcal{D})$ cannot be computed directly, Laplace Approximation (LA) approximates it with

$$q(\theta) = \mathcal{N}(\theta; \theta_{\text{MAP}}, \Sigma), \quad (6)$$

where θ_{MAP} is the maximum a posteriori (MAP) estimate, $\theta_{\text{MAP}} = \arg \max_\theta (\log p(\mathcal{D}|\theta) + \log(p(\theta)))$, and $\Sigma = [-\nabla_\theta^2 (\log p(\mathcal{D}|\theta) + \log p(\theta))|_{\theta = \theta_{\text{MAP}}}]^{-1}$. Two techniques have been proposed to simplify the estimation of Σ . The first technique is Hessian approximations with factorization, and the most lightweight case is a diagonal factorization which ignores off-diagonal elements [30]. The second technique is the subnetwork LA, and the last-layer LA (LLLA) is its special case which only treats the parameters of the last probabilistically [10].

4. Method

As discussed in Sec. 3, the primary goal of our proposed method is to identify diffusion-generated images by exploiting epistemic uncertainty in diffusion. We first briefly explain the learning framework, and then illustrate the process of epistemic uncertainty estimation. Finally, we explain the details of asymmetric learning.

4.1. Overview of Framework

Figure 3 presents the workflow of our proposed method. The framework consists of two main stages: an epistemic uncertainty estimation stage and a training stage. In the uncertainty estimation stage, epistemic uncertainty is estimated in the latent space for each image using a pre-trained diffusion model. The estimated epistemic uncertainty is then prepared for the classifier training. In the training stage, we incorporate the estimated uncertainty with CLIP [46] visual feature motivated by the findings that both visual feature and diffusion measurements are important for generated image detection [5, 38, 44]. Our exploitation of uncertainty is divided into two parts: as a spatial attention map to extract important visual features, and as classification features.

Let $\mathbf{u} \in \mathbb{R}^{HW \times C_1}$ be the spatially aligned epistemic uncertainty and $\mathbf{v} \in \mathbb{R}^{HW \times C_2}$ be the visual feature map. We denote the mean epistemic uncertainty feature by $\bar{\mathbf{u}} \in \mathbb{R}^{1 \times C_1}$, which is the average of \mathbf{u} . We denote the global epistemic uncertainty feature by \mathbf{z}_u , which is simply computed using an attention pooling module on \mathbf{u} . Then the refined visual feature is computed with a multi-head attention module:

$$\mathbf{z}_v = \text{MHA}(\bar{\mathbf{u}}, \mathbf{u}, \mathbf{v}). \quad (7)$$

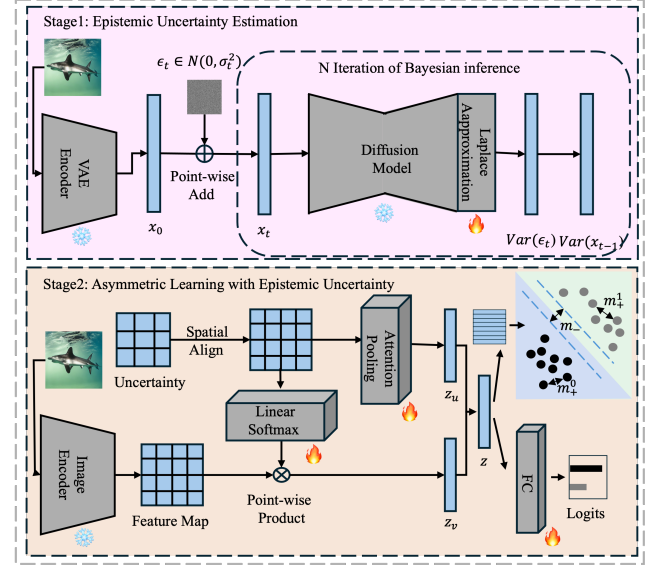


Figure 3. Workflow of our method. In the first stage, we utilize the Laplace approximation to estimate diffusion epistemic uncertainty. In the second stage, we exploit diffusion epistemic uncertainty to train a binary classifier with asymmetric learning.

Finally, \mathbf{z}_u and \mathbf{z}_v are concatenated as the final feature. We train a binary classifier based on this final feature.

4.2. Epistemic Uncertainty Estimation in Diffusion

To estimate diffusion epistemic uncertainty, we perform the forward and reverse diffusion process in the latent space $\mathcal{X} = \{\mathbf{x}^{(i)}\}$ encoded by a pre-trained VAE [26] model, as stated in Sec. 3.1.

Lemma 1. *The epistemic uncertainty in the diffusion model $\epsilon_\theta(\mathbf{x}_t, t)$ is captured by*

$$\begin{aligned} & \text{Var}_{q(\mathbf{x}_{t-1}|\mathbf{x}, t)}(\mathbf{x}_{t-1}) \\ & \times \text{Var}_\theta(\mathbf{E}_\epsilon(\mu_\theta(\sqrt{\alpha_t}\mathbf{x} + (1 - \alpha_t)\epsilon, t))). \end{aligned} \quad (8)$$

By definition, epistemic uncertainty accounts for uncertainty in the model parameters. As stated in Sec. 3.3, to capture variability in the model parameters we build the Bayesian diffusion model by placing a prior distribution $p(\theta)$ over the parameters of a pre-trained diffusion model $\epsilon_\theta(\mathbf{x}_t, t)$. With the inferred posterior $p(\theta|\mathcal{D})$, we can get the predictive distribution of the denoised image at the $(t-1)$ -th step by

$$\begin{aligned} p(\mathbf{x}_{t-1}|\mathbf{x}, t) &= \iint p_\theta(\mathbf{x}_{t-1}|\mathbf{x}_t, \mathbf{x})p(\theta|\mathcal{D})d\theta d\epsilon \\ &= \int p(\theta|\mathcal{D}) \int p_\theta(\mathbf{x}_{t-1}|\mathbf{x}_t, \mathbf{x})d\epsilon d\theta. \end{aligned} \quad (9)$$

As $q(\mathbf{x}_{t-1}|\mathbf{x}_t, \mathbf{x}) \sim \mathcal{N}(\tilde{\mu}_t(\mathbf{x}_t, \mathbf{x}, \tilde{\beta}_t \mathbf{I}))$ [22], we can get

$$\begin{aligned} & \mathbb{E}_\epsilon((\mathbf{x}_{t-1}|\mathbf{x}_t, \mathbf{x})^T(\mathbf{x}_{t-1}|\mathbf{x}_t, \mathbf{x})) \\ & \propto (\mathbb{E}_\epsilon(\mathbf{x}_{t-1}|\mathbf{x}_t, \mathbf{x}))^T(\mathbb{E}_\epsilon(\mathbf{x}_{t-1}|\mathbf{x}_t, \mathbf{x})). \end{aligned} \quad (10)$$

Approximating $\tilde{\mu}_t$ with μ_θ we can get the predict mean via:

$$\mathbb{E}_\theta(\mathbf{x}_{t-1}) = \int p(\theta|\mathcal{D}) \mathbb{E}_\epsilon(\mu_\theta(\sqrt{\alpha_t} \mathbf{x} + (1 - \alpha_t)\epsilon, t)) d\theta. \quad (11)$$

We estimate the second raw moment in the same way:

$$\begin{aligned} & \mathbb{E}_\theta(\mathbf{x}_{t-1}^T \mathbf{x}_{t-1}) \\ &= \int p(\theta|\mathcal{D}) \mathbb{E}_\epsilon((\mu_\theta(\sqrt{\alpha_t} \mathbf{x} + (1 - \alpha_t)\epsilon, t))^T \\ & \quad (\mu_\theta(\sqrt{\alpha_t} \mathbf{x} + (1 - \alpha_t)\epsilon, t))) d\theta \quad (12) \\ & \propto \int p(\theta|\mathcal{D}) (\mathbb{E}_\epsilon(\mu_\theta(\sqrt{\alpha_t} \mathbf{x} + (1 - \alpha_t)\epsilon, t))^T \\ & \quad (\mathbb{E}_\epsilon \mu_\theta(\sqrt{\alpha_t} \mathbf{x} + (1 - \alpha_t)\epsilon, t))) d\theta. \end{aligned}$$

By the law of $\text{Var}(\mathbf{x}) = \mathbb{E}(\mathbf{x}^T \mathbf{x}) - (\mathbb{E}(\mathbf{x}))^T (\mathbb{E}(\mathbf{x}))$, we can get the predictive variance as Eq. (8).

We leverage the LLLA with diagonal factorization to approximate $p(\theta|\mathcal{D})$ as Eq. (6). The Monte Carlo method is used to approximate Eq. (8). We sample model parameters $\theta_i \sim q(\theta) = \mathcal{N}(\theta; \theta_{\text{MAP}}, \Sigma)$ and noise $\epsilon_j \sim \mathcal{N}(0, \mathbf{I})$, where $i = 1, \dots, M$ and $j = 1, \dots, N$. Then epistemic uncertainty is computed as:

$$U(\mathbf{x}_{t-1}|\mathbf{x}, t) = \text{Var}_i(\mathbb{E}_j(\mu_{\theta_i}(\sqrt{\alpha_t} \mathbf{x} + (1 - \alpha_t)\epsilon_j, t))). \quad (13)$$

We choose DDIM as the sampler and set $\sigma_t = 0$ for simplicity, while other samplers, e.g., DDPM, SDE-Solver [51], DPM-Solver [37] is also applicable. Accordingly, we compute μ_{θ_i} as Eq. (4)

4.3. Asymmetric Learning

To learn an even decision boundary with larger margins while preserving the information content of the representation, we propose the Asymmetric Learning (ASL) method.

We employ an asymmetric contrastive loss which maximizes the distance of negative pairs and minimizes the distance of positive pairs by class-specific margins. The loss function is formulated as:

$$\begin{aligned} \ell_m = & \frac{1}{N} \sum_{i=1}^N \mathbb{I}[y_i^{(1)} = y_i^{(2)} = c] \cdot \max(0, m^c - s_W(i)) \\ & + \mathbb{I}[y_i^{(1)} \neq y_i^{(2)}] \cdot \max(0, s_W(i)), \end{aligned} \quad (14)$$

where N is the total number of sample pairs, y_i is the binary label for each sample (0 denotes the real class), $s_W(i)$ is the Cosine similarity between the samples in each pair, m^c is the margin specific to the class c . Characterizing the wide range of features exhibited by the real class presents a significant challenge, making it easier for the model to focus on the simpler artifacts and resulting in a skewed decision boundary [44]. To address this issue, we propose the implementation of a smaller similarity margin specifically

for the real class. The margin for the fake class m^1 is set to 1 by default, which is inherited from the general contrastive loss. We modify m^0 to enhance generalizability.

The overall loss function is a weighted average of cross-entropy loss, asymmetric contrastive loss:

$$\ell(W) = \ell_c(W) + \lambda \ell_m(W), \quad (15)$$

where ℓ_c is the cross-entropy loss, λ is the hyper-parameter controlling the importance of ℓ_m .

5. Experiments

5.1. Datasets and Evaluation Metrics

Following LaRE² [38] and DRCT [5], we performed evaluations on two large-scale datasets: GenImage [63] and DRCT-2M [5]. GenImage comprises 2,681,167 images, segregated into 1,331,167 real and 1,350,000 fake images. GenImage employed all real images from ImageNet [11]. All fake images were generated following the template prompt “photo of [class]”, where “[class]” was substituted by one of 1000 distinct image classes provided in ImageNet. Eight generative models were used for image generation, namely BigGAN [2], GLIDE [43], VQDM [19], Stable Diffusion V1.4&V1.5 [48], ADM [13], Midjourney [42], and Wukong [57]. DRCT-2M consists of two parts: 1,920,000 images generated by various diffusion-based generative models and the real images from MSCOCO [34]. DRCT-2M generated images using two kinds of processes: a text-to-image process covering 10 types of the Stable Diffusion models [48] with prompts derived from MSCOCO and an image-to-image process covering 3 types of Stable Diffusion models and 3 types of ControlNet [60]. We adopted the official division of these two datasets. Following previous works [55], we used accuracy (ACC) with a threshold of 0.5 and average precision (AP) as the metric to evaluate detection performance in our experiments.

5.2. Implementation Details

The proposed method consists of the estimation of DEU and the training of a classifier. To estimate DEU, we used Stable Diffusion V1.5 with a step size of $t = 200$ by default. The prompt was “a photo” for all images. During training and testing phases, the classifier took input images of size 224×224 . CLIP pre-trained ResNet50 [21] was utilized to extract image features. The batch size was set to 48 and the learning rate was set to $1e-4$. We selected λ based on the SDv1.5 subset of GenImage, and set it to 0.5. We found it works well across datasets. All experiments were conducted on NVIDIA Tesla V100 GPUs.

5.3. Comparison with the State of the Arts

We compared our method with several state-of-the-art image generation detection approaches: F3Net [45], GramNet [36], UnivFD [44], DIRE [55], LaRE² [38], and

DRCT DR	Method	Midjourney	SDV1.4	SDV1.5	ADM	GLIDE	Wukong	VQDM	BigGAN	Avg.
w/o	F3Net [ECCV 2020]	55.1	73.1	73.1	66.5	57.8	72.3	62.1	56.5	64.6
	GramNet [CVPR 2020]	58.1	72.8	72.7	58.7	65.3	71.3	57.8	61.2	64.7
	UnivFD [CVPR 2023]	70.1	74.8	75.0	62.9	77.6	72.2	64.8	60.4	69.7
	DIRE [ICCV 2023]	65.0	73.7	73.7	61.9	69.1	74.3	63.4	56.7	67.2
	LaRE ² [CVPR 2024]	66.4	87.3	87.1	66.7	81.3	85.5	84.4	74.0	79.1
	Ours	80.7	89.1	88.6	78.9	88.4	88.1	86.6	83.7	85.6
w/	DRCT/ConvB [ICML 2024]	78.2	97.6	97.1	74.2	75.3	96.0	72.3	67.6	82.3
	DRCT/UniFD [ICML 2024]	83.8	93.1	92.6	83.2	89.5	92.9	91.8	86.0	89.1
	Ours	86.4	96.5	96.2	85.3	94.4	96.2	93.1	84.2	91.5

Table 1. Accuracy (ACC, %) comparisons on GenImage test subsets. Eight models are trained on eight generators respectively. All the eight models are tested on the specified test subsets, and averaging the accuracy scores yields the final results.

DRCT DR	Method	DR	SD Variants					Turbo Variants		LCM Variants			ControlNet Variants			DR Variants			Avg.
			LDM	SDv1.4	SDv1.5	SDv2	SDXL	SD-Turbo	SDXL-Turbo	LCM-SDv1.5	LCM-SDXL	SDv1-Ctrl	SDv2-Ctrl	SDXL-Ctrl	SDv1-DR	SDv2-DR	SDXL-DR		
w/o	F3Net	-	99.9	99.8	99.8	88.7	55.9	87.4	68.3	63.7	97.7	55.0	98.0	72.4	82.0	65.4	50.4	50.3	77.1
	GramNet	-	99.4	99.0	98.8	95.3	62.6	80.7	71.2	69.3	93.1	57.0	90.0	75.6	82.7	51.2	50.0	50.1	76.6
	UnivFD	-	98.3	96.2	96.3	93.8	91.0	93.9	86.4	85.9	90.4	89.0	90.4	81.1	89.1	52.0	51.0	50.5	83.5
	DIRE	SDv1	98.2	99.9	100.0	68.2	53.8	71.9	58.9	54.4	99.8	59.7	99.7	64.2	59.1	52.0	50.0	50.0	71.2
	LaRE ²	SDv1	99.4	100.0	100.0	96.3	97.2	97.6	98.6	86.4	96.1	94.2	96.4	99.2	96.2	49.5	50.6	50.0	88.0
	Ours	SDv1	99.2	99.2	99.2	99.2	99.2	99.1	99.2	99.1	99.2	99.2	99.2	99.2	54.7	53.1	51.1	90.5	
w/	Ours	SDv2	99.2	99.1	99.2	99.4	99.4	99.2	99.3	99.2	99.1	99.2	99.2	99.4	99.4	54.1	51.2	52.2	90.5
	DRCT/Conv-B	SDv1	99.9	99.9	99.9	96.3	83.9	85.6	91.9	70.0	99.7	78.8	99.9	95.0	81.2	99.9	95.4	75.4	90.8
	DRCT/Conv-B	SDv2	99.7	98.6	98.5	99.9	96.1	98.7	99.6	83.3	98.5	93.8	96.7	99.9	97.7	93.9	99.9	90.4	96.6
	DRCT/UniFD	SDv1	96.7	96.3	96.3	94.9	96.2	93.5	93.4	92.9	91.2	95.0	95.6	92.7	92.0	94.1	69.6	57.4	90.5
	DRCT/UniFD	SDv2	94.5	94.4	94.2	95.1	95.6	95.4	94.8	94.5	91.7	95.5	93.9	93.5	93.5	84.3	83.2	67.6	91.4
	Ours	SDv1	99.9	99.9	99.9	99.9	99.9	99.4	99.4	99.9	99.9	99.4	99.4	99.4	99.9	94.2	90.1	98.7	
	Ours	SDv2	99.4	99.7	99.8	100.0	100.0	99.5	99.5	99.3	99.2	99.4	99.9	99.2	95.3	90.1	98.8		

Table 2. Accuracy (ACC, %) comparisons on DRCT-2M. All methods are only trained on SDv1.4 and evaluated on different test subsets on DRCT-2M. For DRCT and our method, we report performance metrics utilizing different diffusion reconstruction model (DR), specifically SDv1 and SDv2.

DRCT [5]. All experimental setups followed the guidelines established by the GenImage [63] and DRCT-2M [5] benchmarks. For the GenImage dataset, we trained a classification model on each of the eight subsets, each corresponding to a different generation method. Each trained model was then evaluated on all eight test subsets. For the DRCT-2M dataset, we trained a classification model on the SDv1.4 subset of DRCT-2M and test it on all the test subsets. A notable distinction in the DRCT's setup is the inclusion of Stable Diffusion inpainting images (referred to as DRCT DR) as hard samples in the training set. To ensure a fair comparison, we aligned the settings and introduced an additional experiment that incorporated images reconstructed using the DRCT inpainting process for a direct comparison with DRCT.

The averaged results over eight trained models on each test subsets of the GenImage dataset are presented in Tab. 1. In the scenario where DRCT DR was not applied, our method outperformed the state-of-the-art by 6.5% in average accuracy (ACC). When integrated with DRCT DR, our method shown an additional gain, outperforming DRCT by 2.4% in average ACC. Similar results are observed on the DRCT-2M dataset, as shown in Tab. 2. Without DRCT DR, our method exceeded the state-of-the-art by achieving a 2.5% increase in average ACC. With DRCT DR, our

method surpassed DRCT by 2.2% in average ACC. The improvements from incorporating DRCT DR were most notable in the DR variant subsets, which were reconstructed from real images using the DRCT inpainting process.

5.4. Generalizability Across Generators

We conducted generalizability comparisons across generators on GenImage and DRCT-2M, respectively.

Comparison on GenImage The results of cross-validation on different training and testing subsets are detailed in Fig. 4. Both LaRE² and our method achieved high accuracy with images that shared the same generation method as the training set. This indicates that detecting generated images from seen generators is relatively straightforward. However, generalizing the detector to unseen generators becomes progressively more challenging as the differences between the generators increase. Compared to LaRE², our method experienced less performance degradation across subsets with different generators, achieving an overall average ACC improvement from 79.1% to 85.6%. Notably, when trained on the BigGAN subset, both methods performed poorly on diffusion-generated images. This suggests a significant distribution gap between images generated by GANs and those produced by diffusion models.

Comparison on DRCT-2M Table 2 reports perfor-

	Test on							
	WuKong	VQDM	BigGAN	Avg.	WuKong	VQDM	BigGAN	Avg.
Train on	SDv1.4	SDv1.5	ADM	GLIDE	SDv1.4	SDv1.5	ADM	GLIDE
MJ	100.0	88.2	88.2	67.1	90.7	77.3	73.6	66.0
SDv1.4	74.0	100.0	99.9	61.7	88.5	100.0	97.2	68.7
SDv1.5	64.8	100.0	100.0	61.9	91.4	100.0	94.6	63.7
ADM	63.4	84.9	83.7	100.0	99.0	90.8	92.0	64.0
GLIDE	59.7	75.5	75.9	74.0	99.8	66.8	71.5	88.7
WuKong	52.8	100.0	99.9	54.0	58.2	100.0	96.3	68.0
VQDM	66.2	99.5	99.4	64.9	72.6	99.1	99.9	72.7
BigGAN	50.0	50.0	50.0	50.0	50.0	50.0	50.0	100.0
Avg.	66.4	87.3	87.1	66.7	81.3	85.5	84.4	74.0
	79.1	80.7	89.1	88.6	79.3	88.4	88.1	86.6
	83.7	85.6	87.1	86.6	83.7	85.6	84.3	85.6

(a) Comparison on ACC. Left: baseline, right: ours.

Figure 4. Results of cross-validation on GenImage. We train eight models on eight subsets respectively, each corresponding to a different generator. For both LaRE² and our method, accuracy (ACC, %) and average precision (AP, %) are reported.

mance comparisons across different test subsets of the DRCT-2M dataset. Consistent with prior observations on GenImage, existing methods achieve excellent performance on seen generators. For unseen generators, methods leveraging diffusion reconstruction error (LaRE²) and those incorporating diffusion-reconstructed images as additional training data (DRCT) show improved performance, particularly when the diffusion models closely resemble those encountered during training. However, a more prevalent and challenging real-world scenario involves detecting images generated by substantially altered and previously unseen diffusion models, such as SDXL, SDXL-Turbo, and LCM-SDXL. Under these conditions, all methods typically exhibit notable performance degradation. In contrast, our proposed method consistently maintains near-perfect detection accuracy across most diffusion-generated image types, except for the DR variants. This robust generalization capability results in an overall improvement in average accuracy from 88.0% to 90.5%.

Like other state-of-the-art methods, our approach initially struggled with DR variants. However, by incorporating DRCT training samples, specifically the DRCT DR images, our method not only successfully overcomes this limitation but also surpasses DRCT by an additional 2.2% in accuracy. This strategic adjustment highlights our method’s adaptability and effectiveness in handling diverse generation scenarios. Moreover, DRCT’s performance significantly depends on the choice of reconstruction models, *i.e.*, SDv1 or SDv2, whereas our method demonstrates substantially improved robustness.

5.5. Generalizability Across Datasets

To further evaluate the generalizability of our proposed method, we conducted cross-dataset experiments following DRCT. Specifically, we trained a classification model on the SDv1.4 subset of DRCT-2M and evaluated it across all subsets of GenImage. The cross-dataset results are summarized in Tab. 3, showing noticeable performance degradation for existing methods. For example, LaRE² achieved

	Test on							
	WuKong	VQDM	BigGAN	Avg.	WuKong	VQDM	BigGAN	Avg.
Train on	SDv1.4	SDv1.5	ADM	GLIDE	SDv1.4	SDv1.5	ADM	GLIDE
MJ	100.0	99.9	99.9	99.0	100.0	99.7	99.8	99.8
SDv1.4	99.1	94.3	94.1	69.1	80.6	92.3	74.6	62.3
SDv1.5	95.3	99.2	98.1	82.3	94.1	98.0	94.2	74.1
ADM	71.5	90.4	89.3	93.2	98.9	88.7	98.5	98.8
GLIDE	66.9	86.8	85.8	84.2	99.0	83.9	90.5	95.5
WuKong	92.3	98.9	98.7	74.3	91.8	98.8	92.0	66.6
VQDM	75.4	94.8	94.7	94.8	97.2	94.2	99.8	98.6
BigGAN	50.0	50.0	50.0	50.0	50.0	50.0	50.0	100.0
Avg.	86.4	87.3	87.1	66.7	81.3	85.5	84.4	74.0
	79.1	80.7	89.1	88.6	79.3	88.4	88.1	86.6
	83.7	85.6	87.1	86.6	83.7	85.6	84.3	85.6

(b) Comparison on AP. Left: baseline, right: ours.

86.2% ACC when trained on the SDv1.4 subset of GenImage (as presented in Fig. 4), but its performance dropped significantly to 53.7% ACC on DRCT-2M (Tab. 3), representing a 32.5% reduction. Similarly, a 34.7% drop in AP (from 99.7% to 65.0%) was observed. Overall, methods based on diffusion reconstruction errors, such as DIRE and LaRE², encountered substantial challenges in maintaining performance across different datasets.

In contrast, our method demonstrated stronger generalization, with smaller declines in both ACC and AP metrics under identical cross-dataset conditions (Tab. 3, Fig. 4). These results underline the advantage of leveraging diffusion epistemic uncertainty, which offers improved robustness across varying image content. Additionally, despite its diffusion focus and orthogonality to unified schemes, DEUA stays competitive and is an effective module in larger frameworks (Sec. A).

5.6. Ablation Study

We performed a series of ablative studies to assess the individual contributions of each component in our model and to examine the impact of various hyperparameters. The overall results of the ablation study for each component are summarized in Tab. 4, which indicates that each element contributed to an independent performance improvement. Additionally, we demonstrate the influence of the sample step in estimating diffusion epistemic uncertainty and the effect of the margin in asymmetric learning, as depicted in Fig. 5.

Influence of Diffusion Epistemic Uncertainty As shown in Tab. 4, integrating diffusion epistemic uncertainty into our model led to the most substantial improvement of 14.2%/8.0% ACC/AP compared to the baseline. The improvement is attributed to the capability of diffusion epistemic uncertainty to capture the general generation properties specific to diffusion models. However, the detection ACC in the BigGAN subset remained relatively low, indicating the intrinsic differences in generation properties between diffusion-based models and GAN-based models.

Influence of Asymmetric Learning The improvements

DRCT DR	Method	Midjourney	SDV1.4	SDV1.5	ADM	GLIDE	Wukong	VQDM	BigGAN	Avg.
w/o	F3Net [ECCV 2020]	71.7/80.4	97.5/99.0	96.7/98.8	55.9/66.1	62.2/74.2	88.1/93.2	62.8/73.1	50.1/50.5	73.2/79.4
	GramNet [CVPR 2020]	70.2/81.3	86.5/92.2	86.1/91.6	52.2/62.5	53.5/65.4	76.3/88.7	54.2/64.6	49.8/50.7	66.1/74.6
	UniFD [CVPR 2023]	73.6/80.1	74.2/84.2	74.2/83.9	56.3/64.2	70.8/80.2	73.3/82.5	56.9/64.8	61.2/72.4	67.6/76.5
	DIRE [ICCV 2023]	52.4/54.6	56.1/60.2	55.7/60.0	50.2/53.2	50.4/56.2	54.2/60.2	49.2/55.4	49.2/52.4	52.2/56.5
	LaRE ² [CVPR 2024]	56.2/71.0	55.1/61.6	54.5/61.5	51.3/65.6	60.4/75.4	53.3/62.0	52.8/65.9	46.1/57.2	53.7/65.0
	Ours	92.2/94.4	97.6/99.1	97.2/99.1	79.4/90.6	90.1/94.2	96.8/98.4	91.4/94.6	71.6/86.1	89.5/94.5
w/	DRCT/Conv-B [ICML 2024]	94.6/98.2	99.6/99.9	99.4/99.9	65.8/78.2	73.2/88.4	99.4/99.9	77.8/89.6	60.4/76.5	83.8/91.3
	DRCT/UniFD [ICML 2024]	86.1/93.2	93.4/97.4	93.2/97.1	74.2/82.3	85.1/90.1	93.2/96.8	89.6/94.2	86.2/91.8	87.6/92.9
	Ours	92.7/95.1	98.1/99.2	97.5/99.2	78.8/90.2	89.7/94.2	97.2/99.2	90.7/94.4	75.8/90.5	90.1/95.3

Table 3. Accuracy (ACC, %) / average precision (AP, %) comparisons of generalizability across datasets. All methods are trained on DRCT-2M/SDV1.4 using SDV1 as the diffusion reconstruction model and evaluated on different testing subsets of GenImage.

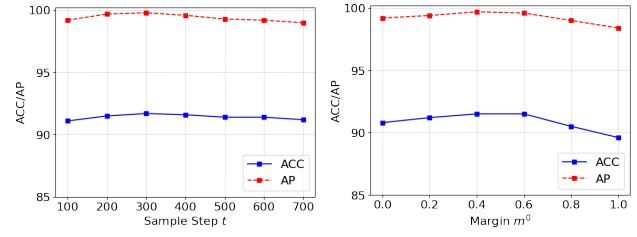
Method	DEU	ASL	Midjourney	SDV1.4	SDV1.5	ADM	GLIDE	Wukong	VQDM	BigGAN	Avg.
A			62.8/82.1	99.9/100.0	99.9/100.0	57.2/88.3	78.4/94.5	99.3/99.9	60.2/88.2	50.8/72.6	76.1/90.7
B	✓		94.1/99.2	99.6/100.0	99.8/100.0	78.5/99.2	91.8/99.6	99.2/99.9	92.8/99.9	66.4/92.1	90.3/98.7
C		✓	71.5/86.2	98.4/99.8	99.2/100.0	64.6/91.5	80.2/94.8	98.2/99.6	68.6/88.2	72.8/90.2	81.7/93.8
D	✓	✓	95.0/99.4	98.7/100.0	99.5/100.0	80.3/99.2	93.0/99.9	98.6/100.0	93.4/100.0	73.6/99.2	91.5/99.7

Table 4. Ablative study results on GenImage test subsets.

brought by asymmetric learning predominantly occurred in subsets generated by models significantly different from those encountered during training. Specifically, asymmetric learning led to substantial performance gains on the BigGAN subset, achieving increases of 22.0% in ACC and 17.6% in AP over the baseline. Recent studies [44] indicate that conventional real-vs-fake classifiers struggle to accurately characterize the real image distribution, causing the real class to act as a “sink class” that aggregates features insufficiently similar to the fake features observed during training. Although diffusion epistemic uncertainty effectively captures intrinsic similarities among diffusion-generated features, it often fails to generalize adequately across diverse generation methods. In contrast, asymmetric learning facilitates the extraction of generic representations, thereby mitigating the “sink class” problem. By integrating diffusion epistemic uncertainty with asymmetric learning, our proposed approach further improved the detection performance, achieving an overall gain of 15.4% in ACC and 9.0% in AP.

Influence of Sample Step As illustrated in Sec. 4.2, we estimate the diffusion epistemic uncertainty through one-step reconstruction process. We set the reconstruction step t to 200 by default following LaRE². Moreover, we conducted experiments to verify the impact of t selection on the performance. The results in Fig. 5a demonstrate our method is relatively robust to t , and using $t \in [100, 400]$ results in comparable performance.

Influence of Margin in Asymmetric Learning Using a relatively smaller margin for the real class is a crucial aspect of the design of asymmetric contrastive learning. To evaluate the impact of different margin values m^0 on performance, we performed experiments and present the results in



(a) Accuracy (ACC, %) / average precision (AP, %) with reconstruction step t range from 100 to 700. (b) Accuracy (ACC, %) / average precision (AP, %) with the real-class margin m^0 range from 0.0 to 1.0.

Figure 5. Influence of sample step t and margin m^0 .

Fig. 5b. As the value of m^0 gradually increased, the average accuracy ACC and AP initially rised, reaching their optimal values at 0.6, and then declined rapidly. As discussed earlier, this is because a heavily compressed feature space struggles to capture the wide range of features exhibited by real-class images, while a properly embedded feature space strikes a balance between separability and generalization.

6. Conclusions

In this work, we propose a novel framework for detecting diffusion-generated images. We observe that recent approaches relying on diffusion reconstruction error as a feature exhibit limited generalizability due to the influence of aleatoric uncertainty inherent in the diffusion process. To address this, we introduce a new feature, diffusion epistemic uncertainty, which quantifies the deviation of an image from the manifold of diffusion-generated images. Experimental results demonstrate that our method achieves state-of-the-art generalizability across a variety of generation methods and datasets.

Acknowledgments

Bing Bai was supported by the Young Elite Scientists Sponsorship Program by CAST under contract No. 2022QNRC001.

References

- [1] Charles Blundell, Julien Cornebise, Koray Kavukcuoglu, and Daan Wierstra. Weight uncertainty in neural network. In *Proceedings of the 32nd International Conference on Machine Learning, ICML 2015, Lille, France, 6-11 July 2015*, pages 1613–1622. JMLR.org, 2015. [2](#)
- [2] Andrew Brock, Jeff Donahue, and Karen Simonyan. Large scale GAN training for high fidelity natural image synthesis. In *7th International Conference on Learning Representations, ICLR 2019, New Orleans, LA, USA, May 6-9, 2019*. OpenReview.net, 2019. [5](#)
- [3] Matthew Chan, Maria Molina, and Chris Metzler. Estimating epistemic and aleatoric uncertainty with a single model. In *Advances in Neural Information Processing Systems 38: Annual Conference on Neural Information Processing Systems 2024, NeurIPS 2024, Vancouver, BC, Canada, December 10 - 15, 2024*, 2024. [1, 2, 3](#)
- [4] Keshigeyan Chandrasegaran, Ngoc-Trung Tran, Alexander Binder, and Ngai-Man Cheung. Discovering transferable forensic features for cnn-generated images detection. In *Computer Vision - ECCV 2022 - 17th European Conference, Tel Aviv, Israel, October 23-27, 2022, Proceedings, Part XV*, pages 671–689. Springer, 2022. [2](#)
- [5] Baoying Chen, Jishen Zeng, Jianquan Yang, and Rui Yang. DRCT: diffusion reconstruction contrastive training towards universal detection of diffusion generated images. In *Forty-first International Conference on Machine Learning, ICML 2024, Vienna, Austria, July 21-27, 2024*. OpenReview.net, 2024. [4, 5, 6](#)
- [6] Riccardo Corvi, Davide Cozzolino, Giovanni Poggi, Koki Nagano, and Luisa Verdoliva. Intriguing properties of synthetic images: from generative adversarial networks to diffusion models. In *IEEE/CVF Conference on Computer Vision and Pattern Recognition, CVPR 2023 - Workshops, Vancouver, BC, Canada, June 17-24, 2023*, pages 973–982. IEEE, 2023. [2](#)
- [7] Riccardo Corvi, Davide Cozzolino, Giada Zingarini, Giovanni Poggi, Koki Nagano, and Luisa Verdoliva. On the detection of synthetic images generated by diffusion models. In *IEEE International Conference on Acoustics, Speech and Signal Processing ICASSP 2023, Rhodes Island, Greece, June 4-10, 2023*, pages 1–5. IEEE, 2023. [2](#)
- [8] Davide Cozzolino, Giovanni Poggi, Riccardo Corvi, Matthias Nießner, and Luisa Verdoliva. Raising the bar of ai-generated image detection with CLIP. In *IEEE/CVF Conference on Computer Vision and Pattern Recognition, CVPR 2024 - Workshops, Seattle, WA, USA, June 17-18, 2024*, pages 4356–4366. IEEE, 2024. [2](#)
- [9] Davide Cozzolino, Giovanni Poggi, Matthias Nießner, and Luisa Verdoliva. Zero-shot detection of ai-generated images. In *Computer Vision - ECCV 2024 - 18th European Conference, Milan, Italy, September 29-October 4, 2024, Proceedings, Part XVIII*, pages 54–72. Springer, 2024. [2](#)
- [10] Erik Daxberger, Agustinus Kristiadi, Alexander Immer, Runa Eschenhagen, Matthias Bauer, and Philipp Hennig. Laplace redux - effortless bayesian deep learning. In *Advances in Neural Information Processing Systems 34: Annual Conference on Neural Information Processing Systems 2021, NeurIPS 2021, December 6-14, 2021, virtual*, pages 20089–20103, 2021. [1, 2, 4](#)
- [11] Jia Deng, Wei Dong, Richard Socher, Li-Jia Li, Kai Li, and Fei-Fei Li. Imagenet: A large-scale hierarchical image database. In *2009 IEEE Computer Society Conference on Computer Vision and Pattern Recognition (CVPR 2009), 20-25 June 2009, Miami, Florida, USA*, pages 248–255. IEEE Computer Society, 2009. [5](#)
- [12] Zhijie Deng, Xiao Yang, Shizhen Xu, Hang Su, and Jun Zhu. Libre: A practical bayesian approach to adversarial detection. In *IEEE Conference on Computer Vision and Pattern Recognition, CVPR 2021, virtual, June 19-25, 2021*, pages 972–982. Computer Vision Foundation / IEEE, 2021. [1](#)
- [13] Prafulla Dhariwal and Alexander Quinn Nichol. Diffusion models beat gans on image synthesis. In *Advances in Neural Information Processing Systems 34: Annual Conference on Neural Information Processing Systems 2021, NeurIPS 2021, December 6-14, 2021, virtual*, pages 8780–8794, 2021. [1, 5](#)
- [14] Hany Farid. Lighting (in)consistency of paint by text. *CoRR*, abs/2207.13744, 2022. [2](#)
- [15] Andrew Y. K. Foong, Yingzhen Li, José Miguel Hernández-Lobato, and Richard E. Turner. 'in-between' uncertainty in bayesian neural networks. *CoRR*, abs/1906.11537, 2019. [2](#)
- [16] Joel Frank, Thorsten Eisenhofer, Lea Schönherr, Asja Fischer, Dorothea Kolossa, and Thorsten Holz. Leveraging frequency analysis for deep fake image recognition. In *Proceedings of the 37th International Conference on Machine Learning, ICML 2020, 13-18 July 2020, Virtual Event*, pages 3247–3258. PMLR, 2020. [2](#)
- [17] Yarin Gal et al. Uncertainty in deep learning. 2016. [2, 3](#)
- [18] Diego Gragnaniello, Davide Cozzolino, Francesco Marra, Giovanni Poggi, and Luisa Verdoliva. Are GAN generated images easy to detect? A critical analysis of the state-of-the-art. In *2021 IEEE International Conference on Multimedia and Expo, ICME 2021, Shenzhen, China, July 5-9, 2021*, pages 1–6. IEEE, 2021. [2](#)
- [19] Shuyang Gu, Dong Chen, Jianmin Bao, Fang Wen, Bo Zhang, Dongdong Chen, Lu Yuan, and Baining Guo. Vector quantized diffusion model for text-to-image synthesis. In *IEEE/CVF Conference on Computer Vision and Pattern Recognition, CVPR 2022, New Orleans, LA, USA, June 18-24, 2022*, pages 10686–10696. IEEE, 2022. [5](#)
- [20] Shuyang Gu, Dong Chen, Jianmin Bao, Fang Wen, Bo Zhang, Dongdong Chen, Lu Yuan, and Baining Guo. Vector quantized diffusion model for text-to-image synthesis. In *IEEE/CVF Conference on Computer Vision and Pattern Recognition, CVPR 2022, New Orleans, LA, USA, June 18-24, 2022*, pages 10686–10696. IEEE, 2022. [1](#)

[21] Kaiming He, Xiangyu Zhang, Shaoqing Ren, and Jian Sun. Deep residual learning for image recognition. In *2016 IEEE Conference on Computer Vision and Pattern Recognition, CVPR 2016, Las Vegas, NV, USA, June 27-30, 2016*, pages 770–778. IEEE Computer Society, 2016. 5

[22] Jonathan Ho, Ajay Jain, and Pieter Abbeel. Denoising diffusion probabilistic models. In *Advances in Neural Information Processing Systems 33: Annual Conference on Neural Information Processing Systems 2020, NeurIPS 2020, December 6-12, 2020, virtual*, 2020. 1, 3, 4

[23] Yingsong Huang, Bing Bai, Shengwei Zhao, Kun Bai, and Fei Wang. Uncertainty-aware learning against label noise on imbalanced datasets. In *Thirty-Sixth AAAI Conference on Artificial Intelligence, AAAI 2022, Thirty-Fourth Conference on Innovative Applications of Artificial Intelligence, IAAI 2022, The Twelfth Symposium on Educational Advances in Artificial Intelligence, EAAI 2022 Virtual Event, February 22 - March 1, 2022*, pages 6960–6969. AAAI Press, 2022. 1

[24] Felix Juefei-Xu, Run Wang, Yihao Huang, Qing Guo, Lei Ma, and Yang Liu. Counteracting malicious deepfakes: Survey, battleground, and horizon. *Int. J. Comput. Vis.*, 130(7):1678–1734, 2022. 1

[25] Alex Kendall and Yarin Gal. What uncertainties do we need in bayesian deep learning for computer vision? In *Advances in Neural Information Processing Systems 30: Annual Conference on Neural Information Processing Systems 2017, December 4-9, 2017, Long Beach, CA, USA*, pages 5574–5584, 2017. 1, 3

[26] Diederik P. Kingma and Max Welling. Auto-encoding variational bayes. In *2nd International Conference on Learning Representations, ICLR 2014, Banff, AB, Canada, April 14-16, 2014, Conference Track Proceedings*, 2014. 4

[27] Siqi Kou, Lei Gan, Dequan Wang, Chongxuan Li, and Zhi-jie Deng. Bayesdiff: Estimating pixel-wise uncertainty in diffusion via bayesian inference. In *The Twelfth International Conference on Learning Representations, ICLR 2024, Vienna, Austria, May 7-11, 2024*. OpenReview.net, 2024. 2

[28] Agustinus Kristiadi, Matthias Hein, and Philipp Hennig. Being bayesian, even just a bit, fixes overconfidence in relu networks. In *Proceedings of the 37th International Conference on Machine Learning, ICML 2020, 13-18 July 2020, Virtual Event*, pages 5436–5446. PMLR, 2020. 1

[29] Balaji Lakshminarayanan, Alexander Pritzel, and Charles Blundell. Simple and scalable predictive uncertainty estimation using deep ensembles. In *Advances in Neural Information Processing Systems 30: Annual Conference on Neural Information Processing Systems 2017, December 4-9, 2017, Long Beach, CA, USA*, pages 6402–6413, 2017. 2

[30] Yann LeCun, John S. Denker, and Sara A. Solla. Optimal brain damage. In *Advances in Neural Information Processing Systems 2, [NIPS Conference, Denver, Colorado, USA, November 27-30, 1989]*, pages 598–605. Morgan Kaufmann, 1989. 4

[31] Jiawei Li, Fanrui Zhang, Jiaying Zhu, Esther Sun, Qiang Zhang, and Zheng-Jun Zha. Forgerygpt: Multimodal large language model for explainable image forgery detection and localization. *CoRR*, abs/2410.10238, 2024. 2

[32] Lingzhi Li, Jianmin Bao, Ting Zhang, Hao Yang, Dong Chen, Fang Wen, and Baining Guo. Face x-ray for more general face forgery detection. In *2020 IEEE/CVF Conference on Computer Vision and Pattern Recognition, CVPR 2020, Seattle, WA, USA, June 13-19, 2020*, pages 5000–5009. IEEE, 2020. 2

[33] Li Lin, Neeraj Gupta, Yue Zhang, Hainan Ren, Chun-Hao Liu, Feng Ding, Xin Wang, Xin Li, Luisa Verdoliva, and Shu Hu. Detecting multimedia generated by large ai models: A survey. *arXiv preprint*, 2024. 2

[34] Tsung-Yi Lin, Michael Maire, Serge J. Belongie, James Hays, Pietro Perona, Deva Ramanan, Piotr Dollár, and C. Lawrence Zitnick. Microsoft COCO: common objects in context. In *Computer Vision - ECCV 2014 - 13th European Conference, Zurich, Switzerland, September 6-12, 2014, Proceedings, Part V*, pages 740–755. Springer, 2014. 5

[35] Huan Liu, Zichang Tan, Chuangchuang Tan, Yunchao Wei, Jingdong Wang, and Yao Zhao. Forgery-aware adaptive transformer for generalizable synthetic image detection. In *IEEE/CVF Conference on Computer Vision and Pattern Recognition, CVPR 2024, Seattle, WA, USA, June 16-22, 2024*, pages 10770–10780. IEEE, 2024. 2

[36] Zhengze Liu, Xiaojuan Qi, and Philip H. S. Torr. Global texture enhancement for fake face detection in the wild. In *2020 IEEE/CVF Conference on Computer Vision and Pattern Recognition, CVPR 2020, Seattle, WA, USA, June 13-19, 2020*, pages 8057–8066. IEEE, 2020. 2, 5

[37] Cheng Lu, Yuhao Zhou, Fan Bao, Jianfei Chen, Chongxuan Li, and Jun Zhu. Dpm-solver: A fast ODE solver for diffusion probabilistic model sampling in around 10 steps. In *Advances in Neural Information Processing Systems 35: Annual Conference on Neural Information Processing Systems 2022, NeurIPS 2022, New Orleans, LA, USA, November 28 - December 9, 2022*, 2022. 5

[38] Yunpeng Luo, Junlong Du, Ke Yan, and Shouhong Ding. Lare²: Latent reconstruction error based method for diffusion-generated image detection. In *IEEE/CVF Conference on Computer Vision and Pattern Recognition, CVPR 2024, Seattle, WA, USA, June 16-22, 2024*, pages 17006–17015. IEEE, 2024. 1, 2, 4, 5

[39] Ruipeng Ma, Jinhao Duan, Fei Kong, Xiaoshuang Shi, and Kaidi Xu. Exposing the fake: Effective diffusion-generated images detection. *CoRR*, abs/2307.06272, 2023. 1, 2

[40] Wesley J. Maddox, Pavel Izmailov, Timur Garipov, Dmitry P. Vetrov, and Andrew Gordon Wilson. A simple baseline for bayesian uncertainty in deep learning. In *Advances in Neural Information Processing Systems 32: Annual Conference on Neural Information Processing Systems 2019, NeurIPS 2019, December 8-14, 2019, Vancouver, BC, Canada*, pages 13132–13143, 2019. 1, 2

[41] Scott McCloskey and Michael Albright. Detecting gan-generated imagery using color cues. *CoRR*, abs/1812.08247, 2018. 2

[42] Midjourney, 2022. 5

[43] Alexander Quinn Nichol, Prafulla Dhariwal, Aditya Ramesh, Pranav Shyam, Pamela Mishkin, Bob McGrew, Ilya

Sutskever, and Mark Chen. GLIDE: towards photorealistic image generation and editing with text-guided diffusion models. In *International Conference on Machine Learning, ICML 2022, 17-23 July 2022, Baltimore, Maryland, USA*, pages 16784–16804. PMLR, 2022. 1, 5

[44] Utkarsh Ojha, Yuheng Li, and Yong Jae Lee. Towards universal fake image detectors that generalize across generative models. In *IEEE/CVF Conference on Computer Vision and Pattern Recognition, CVPR 2023, Vancouver, BC, Canada, June 17-24, 2023*, pages 24480–24489. IEEE, 2023. 2, 4, 5, 8

[45] Yuyang Qian, Guojun Yin, Lu Sheng, Zixuan Chen, and Jing Shao. Thinking in frequency: Face forgery detection by mining frequency-aware clues. In *Computer Vision - ECCV 2020 - 16th European Conference, Glasgow, UK, August 23-28, 2020, Proceedings, Part XII*, pages 86–103. Springer, 2020. 2, 5

[46] Alec Radford, Jong Wook Kim, Chris Hallacy, Aditya Ramesh, Gabriel Goh, Sandhini Agarwal, Girish Sastry, Amanda Askell, Pamela Mishkin, Jack Clark, Gretchen Krueger, and Ilya Sutskever. Learning transferable visual models from natural language supervision. In *Proceedings of the 38th International Conference on Machine Learning, ICML 2021, 18-24 July 2021, Virtual Event*, pages 8748–8763. PMLR, 2021. 4

[47] Hippolyt Ritter, Aleksandar Botev, and David Barber. A scalable laplace approximation for neural networks. In *6th International Conference on Learning Representations, ICLR 2018, Vancouver, BC, Canada, April 30 - May 3, 2018, Conference Track Proceedings*. OpenReview.net, 2018. 2

[48] Robin Rombach, Andreas Blattmann, Dominik Lorenz, Patrick Esser, and Björn Ommer. High-resolution image synthesis with latent diffusion models. In *IEEE/CVF Conference on Computer Vision and Pattern Recognition, CVPR 2022, New Orleans, LA, USA, June 18-24, 2022*, pages 10674–10685. IEEE, 2022. 1, 5

[49] Zeyang Sha, Zheng Li, Ning Yu, and Yang Zhang. DE-FAKE: detection and attribution of fake images generated by text-to-image generation models. In *Proceedings of the 2023 ACM SIGSAC Conference on Computer and Communications Security, CCS 2023, Copenhagen, Denmark, November 26-30, 2023*, pages 3418–3432. ACM, 2023. 2

[50] Jiaming Song, Chenlin Meng, and Stefano Ermon. Denoising diffusion implicit models. In *9th International Conference on Learning Representations, ICLR 2021, Virtual Event, Austria, May 3-7, 2021*. OpenReview.net, 2021. 1, 3

[51] Yang Song, Jascha Sohl-Dickstein, Diederik P. Kingma, Abhishek Kumar, Stefano Ermon, and Ben Poole. Score-based generative modeling through stochastic differential equations. In *9th International Conference on Learning Representations, ICLR 2021, Virtual Event, Austria, May 3-7, 2021*. OpenReview.net, 2021. 5

[52] Chuangchuang Tan, Yao Zhao, Shikui Wei, Guanghua Gu, and Yunchao Wei. Learning on gradients: Generalized artifacts representation for gan-generated images detection. In *IEEE/CVF Conference on Computer Vision and Pattern Recognition, CVPR 2023, Vancouver, BC, Canada, June 17-24, 2023*, pages 12105–12114. IEEE, 2023. 2

[53] Chuangchuang Tan, Huan Liu, Yao Zhao, Shikui Wei, Guanghua Gu, Ping Liu, and Yunchao Wei. Rethinking the up-sampling operations in cnn-based generative network for generalizable deepfake detection. In *IEEE/CVF Conference on Computer Vision and Pattern Recognition, CVPR 2024, Seattle, WA, USA, June 16-22, 2024*, pages 28130–28139. IEEE, 2024. 2

[54] Chuangchuang Tan, Yao Zhao, Shikui Wei, Guanghua Gu, Ping Liu, and Yunchao Wei. Frequency-aware deepfake detection: Improving generalizability through frequency space domain learning. In *Thirty-Eighth AAAI Conference on Artificial Intelligence, AAAI 2024, Thirty-Sixth Conference on Innovative Applications of Artificial Intelligence, IAAI 2024, Fourteenth Symposium on Educational Advances in Artificial Intelligence, EAAI 2014, February 20-27, 2024, Vancouver, Canada*, pages 5052–5060. AAAI Press, 2024. 2

[55] Zhendong Wang, Jianmin Bao, Wengang Zhou, Weilun Wang, Hezhen Hu, Hong Chen, and Houqiang Li. DIRE for diffusion-generated image detection. In *IEEE/CVF International Conference on Computer Vision, ICCV 2023, Paris, France, October 1-6, 2023*, pages 22388–22398. IEEE, 2023. 1, 2, 5

[56] Shiyu Wu, Jing Liu, Jing Li, and Yequan Wang. Few-shot learner generalizes across ai-generated image detection. *CoRR*, abs/2501.08763, 2025. 2

[57] Wukong, 2022. 5

[58] Shilin Yan, Ouxiang Li, Jiayin Cai, Yanbin Hao, Xiaolong Jiang, Yao Hu, and Weidi Xie. A sanity check for ai-generated image detection. 2025. 2

[59] Fan Yang, Ru Zhen, Jianing Wang, Yanhao Zhang, Haoxiang Chen, Haonan Lu, Sicheng Zhao, and Guiguang Ding. HEIE: mllm-based hierarchical explainable AIGC image implausibility evaluator. In *IEEE/CVF Conference on Computer Vision and Pattern Recognition, CVPR 2025, Nashville, TN, USA, June 11-15, 2025*, pages 3856–3866. Computer Vision Foundation / IEEE, 2025. 2

[60] Lvmin Zhang, Anyi Rao, and Maneesh Agrawala. Adding conditional control to text-to-image diffusion models. In *IEEE/CVF International Conference on Computer Vision, ICCV 2023, Paris, France, October 1-6, 2023*, pages 3813–3824. IEEE, 2023. 5

[61] Xu Zhang, Svebor Karaman, and Shih-Fu Chang. Detecting and simulating artifacts in GAN fake images. In *IEEE International Workshop on Information Forensics and Security, WIFS 2019, Delft, The Netherlands, December 9-12, 2019*, pages 1–6. IEEE, 2019. 2

[62] Yichi Zhang and Xiaogang Xu. Diffusion noise feature: Accurate and fast generated image detection. *CoRR*, abs/2312.02625, 2023. 2

[63] Mingjian Zhu, Hanting Chen, Qiangyu Yan, Xudong Huang, Guanyu Lin, Wei Li, Zhijun Tu, Hailin Hu, Jie Hu, and Yunhe Wang. Genimage: A million-scale benchmark for detecting ai-generated image. In *Advances in Neural Information Processing Systems 36: Annual Conference on Neural Information Processing Systems 2023, NeurIPS 2023, New Orleans, LA, USA, December 10 - 16, 2023*, 2023. 5, 6

A. Generalization of DEUA on Diverse Generative Models

Although DEUA is primarily designed for diffusion-based detection and is orthogonal to many unified detection methods, it remains highly competitive with state-of-the-art unified detectors and can serve as a robust component within broader detection frameworks. To comprehensively assess its generalization ability, we further evaluated DEUA on the *UniversalFakeDetect* dataset, which encompasses a diverse set of generative models, including both diffusion and non-diffusion architectures. Under the SDv1.4 setting and leveraging only publicly available pretrained models or code, DEUA achieved competitive or even superior performance compared to existing unified detectors when trained on diffusion models (Tab. 5). These results demonstrate that DEUA not only excels in its targeted domain but also exhibits strong generalizability across a wide spectrum of generative models.

Furthermore, we investigated the robustness of DEUA on novel generative paradigms, such as diffusion transformers and autoregressive models, which represent the latest advancements in image synthesis. As shown in Tab. 6, DEUA consistently maintains high detection accuracy on these emerging architectures, further confirming its adaptability and effectiveness. These findings suggest that, despite being tailored for diffusion-based detection, DEUA possesses the flexibility to handle a broad range of generative models, making it a promising candidate for integration into future unified deepfake detection systems.

Method	Unet		Transformer		Autoregressive		Avg.
	SDv1.4	SDv3	SDv3.5	JanusPRO			
NPR (ProGAN)	76.6	76.2	77.8	76.3	76.7		
FatFormer (ProGAN)	83.2	70.1	65.4	82.6	75.3		
NPR (SDv1.4)	98.2	80.1	83.6	86.5	87.1		
DRCT (SDv1.4)	95.1	91.2	90.4	93.9	92.7		
DEUA (SDv1.4)	99.2	97.3	96.1	98.1	97.7		

Table 6. ACC comparison on new generators. SDv3, sdv3.5 and JanusPRO are collected following GenImage. Results of NPR, FatFormer and DRCT are obtained using their official checkpoints.

Method	GAN						Deep fakes	Low level		Perceptual loss		Guided	LDM				Glide				Dalle	Avg.
	Pro-GAN	Cycle-GAN	Big-GAN	Style-GAN	Gau-GAN	Star-GAN		SITD	SAN	CRN	IMLE		200 steps	200 w/cfg	100 steps	100	50	100	27	27	10	
	NPR (ProGAN)	99.8	95.0	87.6	96.2	86.6	99.8	76.9	66.9	98.6	50.0	50.0	84.6	97.7	98.0	98.2	96.3	97.2	97.4	87.2	87.6	
FatFormer (ProGAN)	99.9	99.3	99.5	97.2	99.4	99.8	93.2	81.1	68.0	69.5	69.5	76.0	98.6	94.9	98.7	94.4	94.7	94.2	98.8	90.9		
NPR (SDv1.4)	57.2	73.8	65.2	66.0	53.5	99.0	52.9	53.0	68.4	48.8	50.8	56.2	92.6	92.9	92.7	90.8	86.4	89.9	69.5	71.6		
DRCT (SDv1.4)	99.6	93.6	87.6	99.2	90.1	99.9	72.3	67.8	60.5	68.2	59.3	92.9	99.8	99.6	99.8	99.8	99.9	99.9	91.2	88.5		
DEUA (SDv1.4)	99.5	94.2	85.3	98.4	90.5	99.5	80.6	72.5	76.4	71.3	74.5	94.8	99.5	99.6	99.9	99.6	99.8	99.8	96.4	91.2		

Table 5. ACC comparisons on the *UniversalFakeDetect* Dataset. Results of NPR, FatFormer and C2P-CLIP trained on ProGAN are from paper C2P-CLIP. Results of NPR and DRCT trained on GenImage SDv1.4 are obtained using their official checkpoints.